Measurement Science
and Technology

PAPER • **OPEN ACCESS**

Comprehensive comparison of distributed and point fibre optic temperature sensors

To cite this article: Xin Lu *et al* 2026 *Meas. Sci. Technol.* **37** 215202

IOP Publishing Meas. Sci. Technol. 37 (2026) 215202 https://doi.org/10.1088/1361-6501/ae6ac2

Measurement Science and Technology

Check for updates

OPEN ACCESS

RECEIVED
10 February 2026

REVISED
10 April 2026

ACCEPTED FOR PUBLICATION
8 May 2026

PUBLISHED
26 May 2026

PAPER

Comprehensive comparison of distributed and point fibre optic temperature sensors

Xin Lu[1,*], Marcus Schukar[1], Kenneth T V Grattan[2], Guillaume Failleau[3] and Stephan Krenek[4]

1 Bundesanstalt für Materialforschung und-prüfung (BAM), Unter den Eichen 87, 12205 Berlin, Germany
2 City St. George's, University of London, Northampton Square, London EC1V 0HB, United Kingdom
3 Laboratoire National de métrologie et d'Essais (LNE), 29 avenue Roger Hennequin, 78197 Trappes, France
4 Physikalisch-Technische Bundesanstalt (PTB) Abbestraβe 2–12, 10587 Berlin, Germany
* Author to whom any correspondence should be addressed.

E-mail: xin.lu@bam.de

Keywords: optical fibre sensing, distributed temperature sensing, measurement uncertainty, quasi-distributed sensing, structural health monitoring

Abstract

Fibre optic sensors offer promising solutions for accurate and precise temperature monitoring across diverse application areas. This study experimentally evaluates the performance of several widely-used fibre optic temperature sensing technologies, including distributed fibre sensing systems based on Raman, Brillouin, and Rayleigh scattering effects, as well as point sensing based on fibre Bragg gratings (FBGs). Under identical thermal conditions, each sensor type is assessed in terms of sensitivity, accuracy, and uncertainty. Distributed measurements are obtained through using Raman optical time domain reflectometry, Brillouin optical time domain analysis, and optical frequency domain reflectometry (OFDR). The results obtained show clear differences in the sensitivity and precision observed, with OFDR and FBGs demonstrating superior stability and repeatability. This comparative analysis, undertaken in this comprehensive way for the first time, offers industry a wealth of foundational data for selecting suitable fibre optic temperature sensors, which can be tailored to their application-specific requirements.

1. Introduction

Fibre optic temperature sensing is a well-known technique that employs optical fibres as both sensing elements and signal transmission media. In such systems, light is launched into the fibre and experiences temperature-induced changes resulting from the changes in the fibre properties, such as refractive index and physical length, creating measurable variations in the optical properties of the light transmitted, such as intensity, polarization, and frequency. By analysing these variations, a calibrated sensing system can be created and then used to retrieve accurately temperature information encoded in the signal [1].

Since the first demonstration of fibre optic temperature sensing, this technology has attracted significant interests due to the wide need in industry for accurate temperature measurements over a wide range and its potentially high sensitivity, coupled to the inherent advantages of optical fibres for many industrial or biomedical measurements, for example, such as small size, chemical inertness, and immunity to electromagnetic interference [2]. Over several decades, major advances in the field have been seen and a wide variety of sensors have been developed, covering an extensive temperature range from just a few K to over 2000 K [3, 4]. These sensors have been, and continue to be deployed in diverse environments, ranging for example from oceanic depths to outer space [5, 6].

Fibre optic temperature sensors are typically categorised into point and distributed types. Point (or discrete) sensors are usually based on specialised fibre structures, such as fibre Bragg gratings (FBGs), Fabry–Pérot (FP) cavities, or Mach–Zehnder interferometers [7–11], amongst several examples, to measure the local temperature accurately and quickly. When properly configured, these sensors usually provide a high signal-to-noise ratio (SNR) and can offer excellent measurement accuracy. The research in this field is continuously progressing e.g. a FP fibre sensor exploiting Vernier effect has been proposed to further enhance sensitivity [12]. Distributed temperature sensing (DTS), by contrast, relies on using standard silica fibres to continuously monitor temperature along the entire fibre length. This approach employs Raman, Brillouin, and Rayleigh scattering effects to extract temperature profiles [13]. Modern DTS systems can achieve temperature uncertainties within a few Kelvin, over distances exceeding 100 km, with spatial resolutions on the order of meters [14]. The point sensor can also employ the large bandwidth by multiplexing several sensing points along the fibre [15]. Such a sensing system can provide accurate measurements at the sensing points but may miss the information located between them. Thus, it is usually called quasi-distributed sensing and has the ability to allow thousands of discrete sensing points to be multiplexed [15]. In practice, the testing requirement and the cost are usually the dominant factors on the selection of different types of fibre temperature sensors.

These types of temperature sensors have found multiple applications in energy-related sectors. For instance, DTS systems are employed to detect leakages in pipelines [16], as well as to monitor critical infrastructure such as nuclear power plants [17]. Additionally, these sensors are extensively used in the oil and gas industry [18]. In addition, they have been applied to monitor the structural health and construction process [19]. With continued technological progress, novel fibre optic temperature sensors keep being proposed and are entering the market. However, the rapid development of such sensors has created a broad selection range for end-users, who may struggle to identify the most suitable sensor type for their specific requirements. As DTS usage grows, many applications require high-precision temperature measurements. For example, the high precision enables early leakage detection or reliable digital-twin development in additive manufacturing. However, the precision values reported in datasheets are difficult to compare across systems, as manufacturers determine them under different and often undisclosed testing conditions. Despite the practical need, to the best of our knowledge no comprehensive comparison of different fibre optic temperature sensors has been reported. Existing comparative studies on DTS technologies based on the three scattering mechanisms focus on very specific application scenarios, such as high rate wells or concrete [20, 21], and consider only a limited set of factors. A broader comparison is therefore necessary and will be highly valuable for both research and industrial applications.

This paper thus aims to deliver a comprehensive evaluation and cross-comparison of the most widely used sensing methods, in terms of key characteristics such as sensitivity, accuracy and measurand uncertainty. This comparison not only can be used to enhance the understanding of their performance and help determine key trade-offs, but also serve as a practical reference for end-users seeking the best sensor solutions available. To the best of our knowledge, this work represents the first systematic evaluation of several fibre optic temperature sensing methods under the controlled conditions discussed. These results provide a quantitative basis for sensor selection and offer significant guidance for high precision measurements across application scenarios such as energy sectors and structural health monitoring.

2. Working principle of different fibre optic temperature sensors

When light is injected into an optical fibre, all three intrinsic scattering mechanisms are simultaneously excited. Each mechanism produces scattered light at distinct spectral offsets relative to the incident optical frequency and exhibits a unique response to environmental perturbations [22], as illustrated in figure 1. This section provides a detailed overview of the working principles underlying various fibre optic temperature sensors.

2.1. Raman based DTS

Raman scattering arises from molecular vibrations within a medium, which lead to a frequency shift in the scattered light relative to the incident light. In standard silica optical fibres, this frequency shift corresponds to a wavelength difference of $\sim$100 nm when the incident light has a wavelength of 1550 nm [23]. It is an inelastic process involving incident photons and phonons in the fibre, where energy exchange results in scattered photons with either increased or decreased energy, corresponding to the Stokes and anti-Stokes components, respectively. The intensity of the components is proportional to the average number of phonons in the medium, which follows Bose–Einstein distribution. As a result, the intensities of the Stokes and anti-Stokes components become temperature dependent and can be expressed as [13]:

$$\begin{cases} I_{\mathrm{as}}(T) \propto \left[\exp\left(\frac{h\nu_{\mathrm{R}}c}{k_{\mathrm{B}}T}\right)-1\right]^{-1} \\ I_{\mathrm{s}}(T) \propto \left[\exp\left(\frac{h\nu_{\mathrm{R}}c}{k_{\mathrm{B}}T}\right)-1\right]^{-1}+1 \end{cases} \tag{1}$$

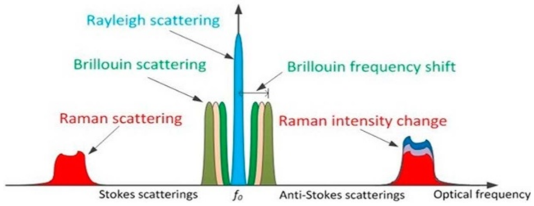

Figure 1. Frequency spectrum of three scattering mechanisms inside an optical fibre. Reproduced from [22].

where h is Planck's constant, c is the speed of light in vacuum, k_B is the Boltzmann constant, T represents temperature, ν_R is the Raman shift, and the subscripts *as* and *s* refer to the anti-Stokes and Stokes bands.

All Raman-based DTS systems exploit this phenomenon by detecting the backscattered signals to extract temperature information along the fibre. However, due to intrinsic fibre attenuation, directly interpreting the received signal intensities can potentially introduce significant error. As a result, modern DTS systems typically rely on the intensity ratio of the Stokes to anti-Stokes components, which mitigates the effect of fibre loss and improves the overall measurement accuracy [13, 23].

2.2. Brillouin based DTS

Brillouin scattering, like Raman scattering, is an inelastic process in which incident photons interact with acoustic phonons in the optical fibre, leading to a frequency shift in the scattered light. This shift, known as the Brillouin frequency shift (BFS), is typically at ∼11 GHz in standard silica fibres when the incident light has a wavelength of 1550 nm [24]. Brillouin-based DTS can be performed by analysing the intensity of the backscattered Stokes and anti-Stokes components, just as in Raman-based systems. Equation (1) describing the intensity of both components can also be applied to spontaneous Brillouin scattering by substituting the Raman shift ν_R with the BFS ν_B [25]. To compensate for the fibre attenuation, the ratio between Rayleigh and Brillouin scattering intensities, called Landau–Placzek ratio, is usually used for temperature measurement [26].

Other than the intensity-based method, Brillouin scattering offers an additional sensing method through direct analysis of the BFS itself. The BFS is linearly dependent on the acoustic velocity of the medium, which varies with temperature, so temperature changes lead to measurable shifts in the BFS. In standard silica fibres, the BFS exhibits a sensitivity of approximately 1 MHz K^{-1} [24, 25].

To determine the local BFS along the fibre, counter-propagating pump and probe beams are usually needed. During the measurement process, the frequency difference between the waves is scanned near the expected BFS. The Brillouin gain spectrum can be constructed based on the optical power change of the probe as a function of the frequency difference. The BFS can then be determined by the peak of this spectrum, corresponding to the point of maximum gain.

2.3. Rayleigh based DTS

Rayleigh scattering occurs when incident light encounters the interfaces of inhomogeneities in the optical fibre. At these interfaces, a small portion of the light is reflected, while the remainder continues to propagate. This scattering process involves no exchange of energy, so it is an elastic process and the optical frequency of the scattered light remains unchanged [25].

For sensing applications, Rayleigh-based systems require a highly coherent light source. Such coherence ensures that the light backscattered within half the pulse length maintains a fixed phase relationship, enabling the detection of interference patterns. Environmental changes, such as temperature and strain variations, can alter the physical property of the fibre, i.e. refractive index and inhomogeneity size, thereby shifting the interference conditions and modifying the detected signal [27, 28]. Therefore, a relationship between the signal change and the environmental variation can be created and this used as the basis of a sensing system.

The influence of temperature variations on the fibre occurs via the thermo-optic effect and thermal expansion, leading to changes in the optical phase of the backscattered signal. These phase changes exhibit a linear dependence on temperature, allowing for precise thermal monitoring [29]. Additionally, environmental variations can lead to measurable shifts in the reflection spectrum, which can also serve as a reliable metric for quantifying temperature changes [30].

2.4. FBG

The FBG is probably the most popular point fibre sensor, one that is being wide used for temperature and strain sensing. A FBG consists of a periodic modulation of the refractive index in the fibre core, constructing a grating that can selectively reflects a narrow band of light while allows other wavelengths to transmit through the structure. The highest reflection occurs at the so-called Bragg wavelength λ_B, expressed as

$$\lambda_B = 2n_{\text{eff}}\Lambda \tag{2}$$

where n_{eff} represents the effective index of the grating and Λ is the grating period [31].

When the temperature varies, the effective index n_{eff} changes via thermo-optic effect and the period Λ changes due to thermal expansion or compression, resulting in a shift of the reflection spectrum. Hence, the temperature variation ΔT can be measured by the Bragg wavelength change $\Delta\lambda_B$, which can be described as [32]

$$\Delta\lambda_B = \lambda_B(\alpha + \xi)\Delta T \tag{3}$$

where α is the thermal expansion of the fibre and ξ represents the thermo-optic coefficient. In practice, light from a broadband source is launched into the grating to obtain the reflection spectrum of a FBG, and λ_B is determined as the centre of the reflection spectrum. As a result, the temperature variation can be determined by the shift of the reflection spectrum that can be simply calculated by the Bragg wavelength change $\Delta\lambda_B$.

It is worth noting that some Rayleigh-based distributed sensing systems operate in a manner similar to FBG sensors. Both rely on detecting reflection spectra resulting from refractive index variations in the fibre core and determine environmental changes through the spectral shift. Therefore, the sensitivity of Rayleigh-based DTS can also be described using equation (3). In other words, when operating at the same wavelength, these two types of fibre temperature sensors exhibit comparable sensitivity. However, the key difference lies in the origin of the refractive index modulation. In FBGs, the index change is intentionally introduced via different techniques for grating writing, whereas in Rayleigh-based DTS it arises randomly during the fibre manufacturing process [33]. As a result, the reflection spectrum of an FBG is regular and symmetric, allowing clear identification of the Bragg wavelength and accurate determination of spectral shifts. By contrast, the reflection spectrum observed in Rayleigh-based DTS has a stochastic profile due to the inherently random index variations along the fibre. This irregular spectral shape complicates the determination of spectral shifts and necessitates advanced signal processing techniques such as cross-correlation and least mean squares fitting [34].

2.5. Multiplexing methods

Distributed fibre sensors utilise backscattered light from the sensing fibre, which can be processed in either the time or frequency domain. For the time domain measurement, optical pulses are sequentially launched into the fibre and the backscattered light is recorded as a function of time. Based on the optical velocity in the fibre, the flight-of-time of the light can be converted into distance. The spatial resolution is equal to the half of the pulse length. Such a sensing system is called optical time domain reflectometry (OTDR), and it can be used to detect the three types of backscattered light by simple optical filtering.

Similarly, the distributed sensing system working in the *frequency* domain is called optical frequency domain reflectometry (OFDR). It employs a laser with a linearly scanned wavelength as the light source. The continuous wave from the laser is split, with one part launched into the sensing fibre for distributed measurements and the other serving as a local oscillator (LO). The light backscattered from the sensing fibre is mixed with the LO, and the beat signal is detected. Due to the flight-of-time of the light travelling along the fibre, the backscattered light exhibits position-dependent frequency shifts relative to the LO. Hence, the distance information can be retrieved from the beat signal by Fourier transformation. The spatial resolution of the OFDR is determined by the wavelength scanning range. While the OFDR system is mainly used for acquiring the Rayleigh backscattering signals, Brillouin- and Raman- based OFDR systems have also been demonstrated for distributed sensing [35, 36].

Several fibre optic point sensors can be multiplexed in one system for quasi-distributed sensing. FBGs with different Bragg wavelengths can be easily multiplexed, as each grating can be identified by its distinct Bragg wavelength. In addition, time-division, code-division and frequency-division multiplexing methods have been proposed to further increase the number of FBGs used in a network [37–39].

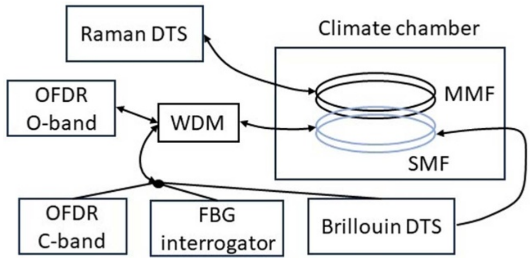

Figure 2. Experimental setup for the sensing performance comparison of various fibre optic temperature sensors.

3. Experimental setup

The experimental setup illustrated in figure 2, is used to evaluate the sensing performance of various fibre optic temperature sensors. Several commercial fibre optic sensing interrogators are employed for this purpose. The Raman-based DTS system operates as an OTDR, involves launching optical pulses at 1064 nm and recording the intensities of the Stokes and anti-Stokes components along the sensing fibre. Due to the inherently weak Raman signal, a ∼30 m long multimode fibre (MMF) is used as the sensing fibre because its large core can collect more scattered light, enhancing the received signal. The MMF has core and cladding diameters of 50 µm and 125 µm, respectively, and is coated with a standard acrylate material. The spatial resolution of the system is set to 1 m, limited by the hardware settings. Even though it is relatively coarse compared to other DTS systems, such a spatial resolution ensures a fair comparison as the Raman-DTS can demonstrate its typical sensing performance with this spatial resolution. Signals are sampled at 0.5 m intervals, and measurements over a 2 min duration are averaged to improve the SNR.

A Brillouin optical time domain analyser (BOTDA) system working at 1550 nm is used here to perform the Brillouin based temperature measurements [40]. This system requires access to both ends of the fibre for launching the pump pulse and probe signals, and is used to acquire the BFS along the entire fibre. In practical deployment, the requirement necessitates arranging the sensing fibre in a loop configuration and limits the maximum sensing range. The frequency scan ranges from 10.7 GHz to 11 GHz in 1 MHz steps. Here, the spatial resolution is 0.2 m with a sampling interval of 0.1 m. The sub-meter resolution is realised by a special technique named pulse pre-pump, that launches a 'pre-pump' pulse into the fibre to excite phonons before the actual pump pulse [41]. In this way, the obtained Brillouin gain spectrum is comparatively narrow even for a short pump pulse, facilitating the BFS determination. Meanwhile, the obtained signal is averaged over 10^{12} times to achieve a satisfactory SNR. According to the datasheet, the sensing performance of this system is consistent with that of standard BOTDA instruments commonly available on the market. Therefore, the results obtained here can be considered representative of typical BOTDA measurements.

Two OFDR systems, operating in the C-band and O-band, are also employed for temperature sensing. The O-band OFDR uses a light source at wavelengths around 1306.6 nm and scans a broad wavelength range to achieve a high spatial resolution of approximately 0.04 mm. The C-band OFDR operates near 1569 nm and achieves the same spatial resolution. To obtain local reflection spectra, the Rayleigh backscattered signal from short fibre segments is transformed into the frequency domain via Fourier transformation. The gauge lengths, determined by the segment length, are 3 cm and 2.5 cm for the O-band and C-band OFDR systems, respectively.

Both the Brillouin DTS and the OFDR systems use a ∼30 m long standard single-mode fibre (SMF) for temperature sensing. The SMF is coated with ∼30 µm thick ORMOCE, a material known to improve sensing performance. A wavelength division multiplexer (WDM), capable of combining light in the C- and O-bands, is used to facilitate simultaneous measurements of the two OFDR systems. Additionally, the C-band input of the WDM provides the access for the SMF to the Brillouin DTS and an FBG interrogator, whereby the three sensing systems (OFDR at C-band, Brillouin DTS and FBG interrogator) are connected alternatively to this input to conduct corresponding temperature measurements.

Although various DTS techniques exist, it is both impractical and unnecessary to compare all of them, as techniques based on the same scattering mechanism generally exhibit very similar sensing performance. Therefore, following the approach in [20, 21], we select Raman-OTDR, BOTDA, and OFDR as representative methods, one from each scattering-based category. These techniques also operate in either the time or frequency domain, allowing the comparison to provide additional insight into the two interrogation approaches.

The SMF used contains two FBGs, which were written during the fibre drawing process. Each grating is 8 mm long and spaced 2 m apart. The 2 m spacing is selected to ensure it exceeded the largest spatial resolution of the used DTS systems. At room temperature, the Bragg wavelengths are 1548 nm and 1550 m, respectively. The FBG interrogator emits a broadband light source spanning between 1510 nm and 1590 nm and records the reflection spectrum with a 5 pm resolution.

Except for Raman based DTS, all sensing methods used in this study have the well-known cross sensitivity to both temperature and strain. Thereby, thermal expansion or contraction of the fibre coating can impose a thermally induced strain on the fibre, contributing to the measured signal. This interaction effectively alters the apparent temperature sensitivity of the sensing systems [42–44].

The SMF and MMF used are loosely coiled to a diameter of ∼16 cm and positioned at the centre of a climate chamber. Bending-induced differential loss is negligible in our experiment because the sensing fibre is coiled with a large diameter, preventing micro-bending effects that can otherwise distort the Stokes/anti-Stokes ratio. The temperature inside the chamber is increased from 20 °C to 80 °C with a 20 °C step. The chamber maintains a temperature stability of ±0.3 °C and offers a temperature-setting resolution of 0.1 °C. Most of the MMF is used for sensing, but only ∼5 m of the SMF, including the two FBGs, is positioned inside the chamber. Each temperature step lasts one hour to allow for stabilization and to perform all the measurements. Distributed measurements are repeated five times for each temperature step, while the FBG interrogator records data at 100 Hz. The repetition number is selected as the best compromise between achieving statistically meaningful analysis and minimizing long duration effects such as system drift and changes in the climate chamber conditions. The relative humidity is maintained at 50% to eliminate the potential influence of moisture on the temperature readings [44, 45].

4. Experimental results and discussion

4.1. Detected signal change at different temperatures

As described in section 2, the signals detected by different fibre optic sensing systems respond differently to temperature variations. According to equation (1), the intensities of the anti-Stokes and Stokes components in Raman scattering increase with temperature. These components are recorded separately along the sensing fibre at various temperatures, and their ratio I_{as}/I_s is usually used to suppress the effects of fibre attenuation. Figure 2(a) presents the averaged intensity ratios along the sensing fibre for different temperatures. The intensity ratio clearly increases with temperature, but noticeable non-uniformity appears at higher temperatures, indicating uneven measurement along the fibre. Further explanation of this phenomenon is provided in section 4.3.

In figure 3(b), the BFSs along the fibre are plotted for various temperatures. The 5 m long fibre segment between length of approximately 12 m and 17 m experiences temperature changes in the climate chamber, resulting in an upward shift in the local BFS. The rest of the fibre, located outside the chamber at room temperature, shows minimal variation. At around 13 m, the sensing system fails to retrieve the BFS due to the FBG2. This grating actually affects Brillouin sensing across the entire fibre, as its Bragg wavelength is deliberately set to 1550 nm that coincides with the operating wavelength of the Brillouin DTS. This results in reflection of both the pump and probe lightwaves, reducing the local SNR so much that it is impossible to retrieve the BFS around the grating. Meanwhile the Brillouin measurement over the entire fibre is affected because either pump or probe is attenuated, thus the blue curve corresponding to 20 °C displays multiple spurious spikes, indicating inaccurate BFS determination. At higher temperatures, the reflection spectrum of FBG2 shifts away from the operating wavelength of the Brillouin DTS, allowing the sensing system to function properly. The improved SNR at higher temperatures suppresses most of these artefacts, as shown in figure 3(b). However, the sidelobes of the reflection spectrum still affects the BFS retrieval near the grating, and hence the BFS is still missing at this region.

Figures 3(c) and (d) display the spectral shifts measured by the OFDR systems operating in the O- and C-bands, respectively. The measurement at 20 °C serves as the reference, resulting in a baseline shift of approximately 0 GHz. Curves corresponding to higher temperatures reflect offsets from this baseline. Only the fibre segment located inside the climate chamber is shown, to emphasise the details in the results. At higher temperatures, such as 60 °C and 80 °C, the fibre coil experiences thermal expansion, inducing strain variations along loops that can be captured by the OFDR systems. This effect manifests as periodic ripples in the measured shift profiles.

The inherent inhomogeneity in the fibre properties, e.g. refractive index fluctuations, and coating thickness variations, and measurement noise lead to non-uniform thermal responses along the sensing

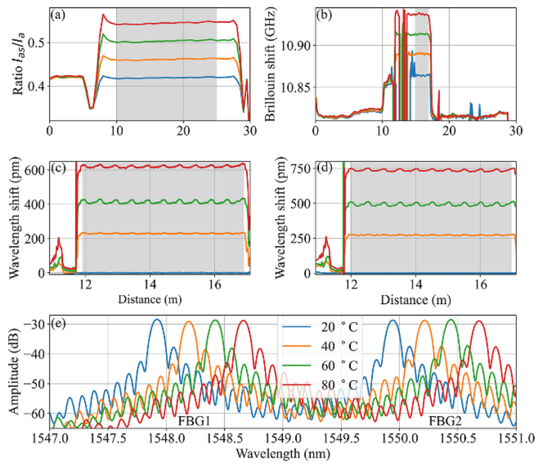

Figure 3. Measurement results of (a) Raman-based DTS, (b) Brillouin-based DTS, (c) OFDR working at O-band, (d) OFDR working at C-band, (e) two FBG sensors. The data in the shaded region is used for statistical analysis.

fibres. This results in spatial variability in the DTS outputs, as seen in figures 3(a)–(d). To minimise the impact of these variations and ensure the reliability of the subsequent sensitivity and uncertainty analysis, only data within the shaded regions of each plot is considered.

The reflection spectra of the two FBGs are simultaneously recorded by a single interrogator. Figure 3(e) presents the spectra averaged across different temperatures. The spectra exhibit low reflection peaks and ripple structures, which are characteristic of such gratings [46]. Most importantly, the spectra exhibit a redshift (i.e. towards longer wavelengths), with increasing temperature, and the temperature determination can be realised by tracking the spectral peak of each FBG.

4.2. Temperature sensitivity

As explained in section 2, the temperature information can be retrieved from different optical properties. For example, with Raman DTS, the intensity ratio $I_{\mathrm{as}}/I_{\mathrm{s}}$ is used, expressed as

$$\frac{I_{\mathrm{as}}}{I_{\mathrm{s}}} \propto \exp\left(-\frac{h\nu_{\mathrm{R}}c}{k_{\mathrm{B}}T}\right) \qquad \ln\frac{I_{\mathrm{as}}}{I_{\mathrm{s}}} \propto -\frac{h\nu_{\mathrm{R}}c}{k_{\mathrm{B}}T}. \tag{4}$$

Hence, the temperature is proportional to the natural logarithm of the intensity ratio $\ln(I_{\mathrm{as}}/I_{\mathrm{s}})$. This logarithmic ratio is calculated along the sensing fibre and averaged over the range from 10 m to 25 m, corresponding to the shaded region in figure 3(a), for each temperature setting. The resulting averaged values are presented as data points in figure 4(a). Similarly, the BFS and Rayleigh-based spectral shifts, averaged over their respective shaded regions, are plotted in figures 4(b) and (c) for the Brillouin DTS and OFDR measurements, respectively. The Bragg wavelengths corresponding to the two FBGs are shown as a function of temperature in figure 4(d).

According to equation (3), the temperature sensitivity of the OFDR measurement increases with the operating wavelength. The C-band OFDR operates at a wavelength approximately 1.201 times greater than that of the O-band system, closely matching the ratio of the observed sensitivities (12.14/10.23 $\approx$ 1.187). The minor deviation between these values may result from the wavelength dependence of the thermo-optic coefficient [47]. Furthermore, a comparison between figures 4(c) and (d) confirms that the OFDR and the FBG exhibit the same sensitivity when operating at the same wavelength.

4.3. Temperature accuracy

Based on the linear fittings presented in figure 4, the signals obtained from various DTS methods are converted into temperature profiles along the fibre and are shown in figure 5. To highlight the detailed trends, only the fibre segments located inside the climate chamber are displayed. Overall, all DTS methods demonstrated reliable temperature measurement capabilities. The temperature measured by the Raman-based DTS along the MMF closely matches the thermal conditions within the chamber, as shown in figure 5(a). However, the logarithmic intensity ratio $\ln(I_{\mathrm{as}}/I_{\mathrm{s}})$ varies along the fibre, limiting high-accuracy temperature determination to localised regions.

For instance, the results between 10 m and 15 m align well with the set temperatures of 40 °C and 60 °C, while those at other thermal conditions are underestimated. Conversely, measurements from

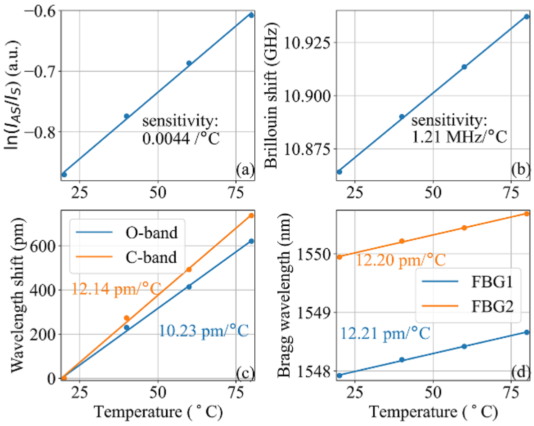

Figure 4. Temperature sensitivity summary of (a) Raman-based DTS, (b) Brillouin-based DTS, (c) OFDR, and (d) FBG sensors. Dots are experimental results and solid lines represent the linear fitting.

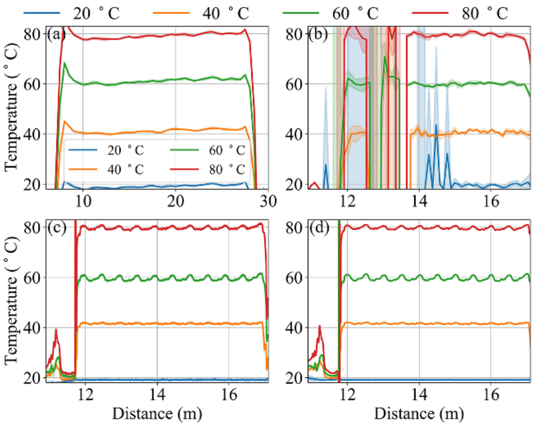

Figure 5. Temperature profiles along the sensing fibre obtained by (a) Raman-based DTS, (b) Brillouin-based DTS, (c) OFDR at O-band, and (d) OFDR at C-band. Solid lines are the retrieved temperature and the shaded regions around the lines represent measurement uncertainty.

20 m to 25 m accurately reflect the set points of 20 °C and 80 °C, but overestimate the remaining temperatures. The observed non-uniformity in $\ln(I_{as}/I_s)$ is so large that it cannot be attributed solely to variations in fibre properties. Instead, it arises likely from a combination of detector noise, mode coupling within the fibre, and attenuation along the MMF coil, particularly at an incident wavelength of 1064 nm. Additionally, ageing of system components may contribute to this effect.

The temperature profile obtained from the Brillouin DTS is presented in figure 5(b). Compared to the Raman-based measurement, the result is more uniform along the fibre, with minor variations likely to be attributed to measurement noise. The measured temperatures closely match the set values within the climate chamber. Additionally, figure 5(b) clearly reveals the presence of the FBGs between 12 m and 14 m, where the BFS could not be determined. The periodic modulation of the refractive index within the gratings disrupts the Brillouin gain spectrum, preventing accurate retrieval of the BFS in that region.

The shaded area around each solid line represents the temperature uncertainty along the fibre, calculated as the standard deviation from five repeated measurements. Although uncertainty is plotted in all subfigures of figure 5, it is visible only in figure 5(b), indicating that the Brillouin DTS exhibits the largest measurement uncertainty. A detailed comparison is provided in section 4.4.

The temperature profiles measured by the OFDR systems operating at the O- and C-bands are shown in figures 5(c) and (d), respectively. At lower temperatures, both profiles are highly uniform. However, at higher temperatures, periodic variations appear along the fibre, caused by thermally induced strain in the coiled fibre loops. This strain affects the linear fitting process, leading to noticeable deviations and reduced accuracy at the lower temperature setpoints of 20 °C and 40 °C. The periodic temperature variations shown in figures 5(c) and (d) would be absent in a straight fibre.

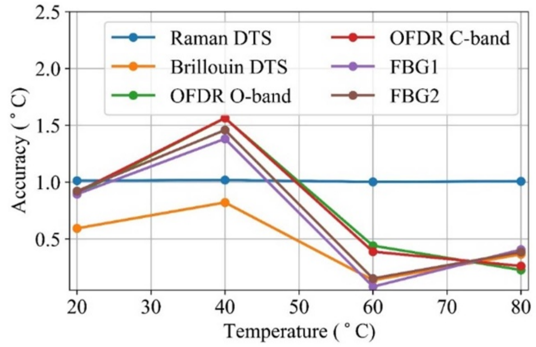

Figure 6. Temperature accuracy obtained by different fibre optic sensing methods at different temperatures.

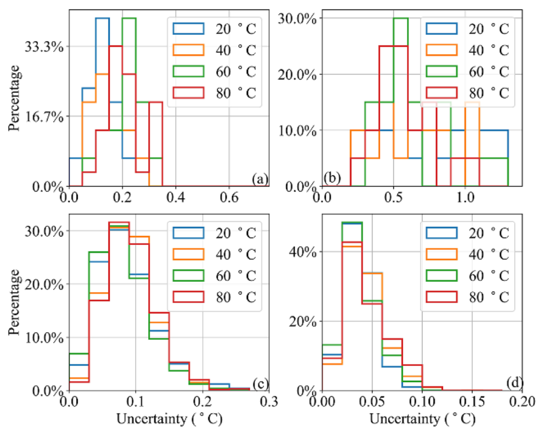

Figure 7. Histogram of temperature uncertainties obtained by (a) Raman-based DTS, (b) Brillouin-based DTS, (c) OFDR at O-band, and (d) OFDR at C-band.

In the same manner, the Bragg wavelengths of the two FBGs can be converted into temperature values, allowing the measurement accuracy to be assessed as the difference between the measured and actual temperatures. For the DTS methods, the measured temperature within the grey-shaded region is first averaged, and the deviation from the corresponding set temperature is taken as the measurement accuracy. The computed accuracies under various thermal conditions are summarised in figure 6. It is evident that the Raman DTS exhibits the lowest accuracy, with an error of approximately 1 °C, whereas the other sensing methods achieve significantly better accuracy, well below 1 °C, particularly at higher temperatures. All sensing systems show the largest deviation at 40 °C, which is likely attributable to a systematic error associated with the climate chamber.

4.4. Temperature uncertainty comparison

As discussed, measurement uncertainty is another critical parameter in fibre optic sensing, alongside sensitivity and accuracy. In this paper, uncertainty is defined as the standard deviation of repeated measurements, representing the precision of the sensing system. Ultimately, the uncertainty is governed by the SNR of the system. In distributed and quasi-distributed sensing configurations, the SNR typically degrades with increasing sensing distance, mainly due to fibre attenuation. Additionally, localised conditions, for example variations in fibre properties or environmental influences, can further impact uncertainty at specific positions, as illustrated in figure 5(b).

Therefore, the uncertainties of the DTS measurements have been analysed statistically. At each sampling point within the shaded regions shown in figure 3, the standard deviation is calculated from five repeated measurements. These uncertainties are presented as histograms in figure 7 for each sensing method. Since the shaded regions span different fibre lengths and the DTS methods differ in spatial sampling, the total number of sampling points used for statistical analysis varies across methods. To enable meaningful comparison, the *y*-axis of each histogram is normalised to reflect the percentage of occurrences per bin, rather than absolute counts.

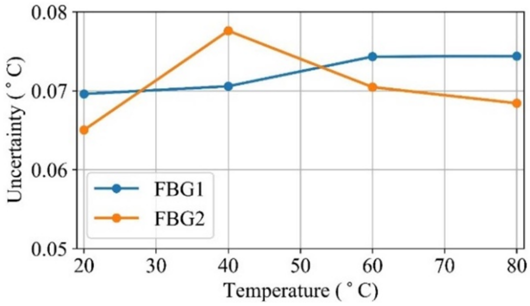

Figure 8. Temperature uncertainties obtained by two FBGs at different temperatures.

According to figure 7(a), the uncertainty of the Raman DTS system over a 30 m sensing distance can be estimated at approximately 0.6 °C, as most sampling points exhibit a standard deviation below this value. At 20 °C, the uncertainty is below 0.5 °C, but the upper limit slightly increases with temperature. By contrast, the Brillouin DTS system demonstrates the highest uncertainty, exceeding 1 °C, as shown in figure 7(b). Two factors are believed to contribute to this performance degradation. First, FBG2 has a reflection spectrum near the operating wavelength of the system, causing partial reflection of both pump and probe signals, thus reducing the SNR. Second, the system operates at a spatial resolution of 20 cm, significantly finer than the typical 1 m resolution of standard Brillouin sensors. Even though the pulse pre-pump method is used, the sub-meter spatial resolution leads to lower SNR and a broader Brillouin gain spectrum, deteriorating accurate BFS determination and increasing measurement uncertainty [40].

The histogram profiles for the Raman and Brillouin DTS appear unstable and fluctuate with temperature, which can be attributed to the limited number of sampling points: 30 for Raman and 20 for Brillouin, used in the statistical analysis. With a larger dataset, these profiles would be expected to stabilise and become less temperature-dependent.

By contrast, the histogram profiles for the OFDR measurements shown as histograms in figures 7(c)–(d) are consistent across different temperatures due to the large number of sampling points (∼1000) used in the analysis. Both OFDR systems exhibit high measurement precision, with uncertainties around 0.2 °C. The C-band OFDR performs even better, showing uncertainty below 0.1 °C for most sampling points, and frequently achieving ⩽0.05 °C. This superior performance is partly due to the higher sensitivity of the system. Temperature uncertainty can be calculated by dividing the standard deviation of the wavelength shift by the sensitivity. As discussed previously, the C-band OFDR has a higher sensitivity as it operates at a longer wavelength, and, consequently, has a lower uncertainty. Additionally, the O-band OFDR is manufactured approximately five years earlier than the C-band system, which may also contribute to its relatively higher uncertainty.

The FBGs are used to measure the temperature only at the fixed positions, and the measurement is very fast, unlike the DTS measurements that require frequency scanning and/or signal averaging. Thus 88 individual FBG measurements at each temperature are used together to determine the uncertainty, and the results are shown in figure 8. The two FBGs have almost the same uncertainty around 0.07 °C at different test temperatures, which are limited by several factors of the FBG interrogator such as the spectral resolution, SNR and algorithm to determine the Bragg wavelength. It means the FBG measurement offers a more precise result than the Raman and Brillouin based DTS methods. This is understandable because the FBG used, although written as a very weak grating, still has a larger reflectivity than the spontaneous scattering effects. In addition, the FBG has a larger sensitivity than the two distributed sensing methods, as shown in figure 4. The FBG sensor demonstrates a similar uncertainty as the OFDR system because they share the same working principle. Although the Rayleigh backscattering coefficient is much lower than the FBG reflection, the OFDR system employs coherent detection to acquire the backscattered light, so a high SNR is guaranteed, resulting in a small resultant temperature uncertainty.

As a summary, the key testing results of the different sensor systems are presented in table 1. As discussed above, the uncertainty and accuracy of the DTS systems vary with both distance and temperature. To provide a representative comparison, the values reported in the table are averaged over the region of interest (as indicated in figure 3) and across all tested temperatures. The corresponding averaged values for the two FBG sensors are also included.

Both the OFDR method and the FBG sensors exhibit similarly high sensitivity, as they share the same underlying measurement principle. In addition, the OFDR system demonstrates the lowest uncertainty and excellent accuracy, surpassing even the FBG sensors, because the listed parameters

Table 1. Comparison of key sensing parameters of the tested fibre temperature sensors.

	Spatial resolution	Sensitivity	Uncertainty	Accuracy
Raman	1 m	4.4×10^{-3} °C^{-1}	0.37 °C	1.01 °C
Brillouin	0.2 m	1.21 MHz °C^{-1}	0.70 °C	0.48 °C
Rayleigh (O)	0.03 m	10.26 pm °C^{-1}	0.09 °C	0.78 °C
Rayleigh (C)	0.025 m	12.14 pm °C^{-1}	0.04 °C	0.78 °C
FBG	—	12.21 pm °C^{-1}	0.14 °C	1.42 °C

represent the average of approximately 1000 sensing points along the fibre. This averaging process effectively reduces measurement noise and mitigates the influence of fibre non uniformity.

5. Conclusion

In this paper, a comprehensive cross-comparison of distributed and point fibre optic temperature sensors in terms of the key parameters of sensitivity, accuracy, and measurement uncertainty is presented. DTS methods based on Raman, Brillouin, and Rayleigh scattering effects, and FBGs (the most widely used point sensor type), were evaluated under identical thermal conditions. A SMF with gratings written into it is used for Brillouin-, Rayleigh-based and FBG measurements to ensure a consistent basis for a high-quality comparison. Experimental results obtained have revealed that FBG and OFDR sensors exhibit comparable performance, mainly due to their high sensitivity and the shared operating principles. In contrast, the Raman- and Brillouin-based DTS systems have demonstrated relatively lower sensitivity and higher uncertainty. To the best of our knowledge, this work represents the first systematic evaluation of several fibre optic temperature sensing methods under controlled laboratory conditions. However, real-world environments are far more complex and the sensors face practical challenges such as bending loss and cross-sensitivity. Thus it is essential to investigate these factors in future work to provide end-users with practical guidance for sensor selection based on performance metrics. As the range of application scenarios continues to expand, the performance requirements for DTS systems are becoming increasingly stringent and diverse. These sensors are expected to enable multi parameter measurements and to maintain reliable operation in harsh environments, including high temperatures, intense radiation, or chemically corrosive conditions. Future work will extend this comparison to a broader set of operating conditions to provide targeted guidance for sensor selection in these demanding and extreme environments.

Acknowledgments

The project 22IEM07 INFOTherm has received funding from the European Partnership on Metrology, co-financed from the European Union's Horizon Europe Research and Innovation Programme and by the Participating States.

Data availability statement

The data cannot be made publicly available upon publication because they are not available in a format that is sufficiently accessible or reusable by other researchers. The data that support the findings of this study are available upon reasonable request from the authors.

Author contributions

Xin Lu 0000-0003-1447-3717
Conceptualization (equal), Methodology (equal), Visualization (equal), Writing – original draft (equal), Writing – review & editing (equal)

Marcus Schukar 0009-0006-6411-1094
Conceptualization (equal), Methodology (equal), Writing – original draft (equal), Writing – review & editing (equal)

Kenneth T V Grattan
Writing – original draft (equal), Writing – review & editing (equal)

Guillaume Failleau
Writing – original draft (equal), Writing – review & editing (equal)

Stephan Krenek 0000-0001-9289-044X
Funding acquisition (equal), Project administration (equal), Writing – review & editing (equal)

References

[1] Gangwar R, Kumari S, Pathak A, Gutlapalli S and Meena M 2023 Optical fiber based temperature sensors: a review *Optics* **4** 171–97
[2] Deng T and Jiang J 2022 Optical fiber sensors in extreme temperature and radiation environments: a review *IEEE Sens. J.* **22** 13811–34
[3] Rajini-Kumar R, Suesser M, Narayankhedkar K, Krieg G and Atrey M 2008 Performance evaluation of metal-coated fiber Bragg grating sensors for sensing cryogenic temperature *Cryogenics* **48** 142–7
[4] Habisreuther T, Elsmann T, Pan Z, Graf A, Willsch E and Schmidt M 2015 Sapphire fiber Bragg gratings for high temperature and dynamic temperature diagnostics *Appl. Therm. Eng.* **91** 860–5
[5] Wang L, Wang Y, Song S and Li F 2021 Overview of fibre optic sensing technology in the field of physical ocean observation *Front. Phys.* **9** 745487
[6] Abad S, Araujo F, Pinto F, González Torres J, Rodriguez R and Moreno M 2017 Fiber optic sensing subsystem for temperature monitoring in space in-flight applications *Proc. SPIE* **10563** 105631D
[7] Wang H, Chen C, Ni Y, Jayawickrema M and Epaarachichi J 2023 Computer-aided feature recognition of CFRP plates based on real-time strain fields reflected from FBG measured signals *Composites B* **263** 110866
[8] Wang H, Xiang P and Jiang L 2019 Strain transfer theory of industralized optical fiber-based senors in civil engineering: a review on measurement accuracy, design and calibration *Sens. Actuators A* **285** 414–26
[9] Wang H, Dai J and Wang X 2021 Improved temperature compensation of fiber Bragg grating-based sensors applied to structures under different loading conditions *Opt. Fiber Technol.* **63** 102506
[10] Liu H, Peng N, Meng W, Zhou Z, Liu Q and Xie S 2024 Optical fiber temperature sensing probe based on F–P cavity for human body temperature monitoring *IEEE Sens. J.* **24** 16188–95
[11] Hu X, Shen X, Wu J, Peng J, Yang L, Li J, Li H and Dai N 2016 All fiber M-Z interferometer for high temperature sensing based on a hetero-structured cladding solid-core photonic bandgap fiber *Opt. Express* **24** 21693–9
[12] Wang Z, Rajan G, Wang Z, Rout A and Jibon R 2026 High-sensitivity fiber optic temperature sensor based on Vernier effect in a polymethyl methacrylate capillary and barium titanate microsphere *Meas. Sci. Technol.* **37** 045103
[13] Hartog A H 2017 *An Introduction to Distributed Optical Fibre Sensors* (https://doi.org/10.1201/9781315119014)
[14] Lu P, Lalam N, Badar M, Liu B, Chorpening B, Buric M and Ohodnicki P 2019 Distributed optical fiber sensing: review and perspective *Appl. Phys. Rev.* **6** 041302
[15] Li C, Tang J, Cheng C, Cai L and Yang M 2021 FBG arrays for quasi-distributed sensing: a review *Photon. Sens.* **11** 91–108
[16] Li H, Zhu H, Tan D, Shi B and Yin J 2023 Detecting pipeline leakage using active distributed temperature sensing: theoretical modeling and experimental verification *Tunn. Undergr. Space Technol.* **135** 105065
[17] Kim B, Kim Y, Lee Y, Nam K, Yoon J, Shin Y, Kim H, Lee J and Lee B 2024 Experimental study on practical application of optical fiber sensor (OFS) for high-temperature system *Nucl. Eng. Technol.* **56** 5182–9
[18] Ashry I, Mao Y, Wang B, Hveding F, Bukhamsin A, Ng T and Ooi B 2022 A review of distributed fiber–optic sensing in the oil and gas industry *J. Lightwave Technol.* **40** 1407–31
[19] Tian W, Zhu H, Liu Z, Huang C, Zheng J and Yang H 2023 Measuring height of poured concrete via fiber-optic temperature sensing *Meas. Sci. Technol.* **34** 115202
[20] Seabrook B C, Ellmauthaler A, LeBlanc M, Jaaskelainen M, Maida J L and Wilson G A 2022 Comparison of Raman, Brillouin, and Rayleigh distributed temperature measurements in high-rate wells *Petrophysics* **63** 685–99
[21] Delepine-Lesoille S, Planes I, Landolt M, Hermand G and Perrochon O 2017 Compared performances of Rayleigh, Raman, and Brillouin distributed temperature measurements during concrete container fire test *Proc. SPIE* **10323** 103236G
[22] Lu X, Thomas J P and Hellevang O J 2019 A review of methods for fibre-optic distributed chemical sensing *Sensors* **19** 2876
[23] Li L and Zhang M 2022 Physics and applications of Raman distributed optical fiber sensing *Light Sci. Appl.* **11** 128
[24] Motil A, Bergman A and Tur M 2016 [INVITED] State of the art of Brillouin fiber-optic distributed sensing *Opt. Laser Technol.* **78** 81–103
[25] Thévenaz L 2011 *Advanced Fiber Optics: Concepts and Technology* (EPFL Press)
[26] Wait P and Newson T 1996 Landau Placzek ratio applied to distributed fibre sensing *Opt. Commun.* **122** 141–6
[27] Lu X and Thomas P 2020 Numerical modeling of Fcy OTDR sensing using a refractive index perturbation approach *J. Lightwave Technol.* **38** 974–80
[28] Ding Z, Guo H, Liu K, Hua P, Zhang T, Li S, Liu J, Jiang J and Liu T 2023 Advances in distributed optical fiber sensors based on optical frequency-domain reflectometry: a review *IEEE Sens. J.* **23** 26925–41
[29] Nikitin S, Kuzmenkov A, Gorbulenko V, Nanii O and Treshchikov V 2018 Distributed temperature sensor based on a phase-sensitive optical time-domain Rayleigh reflectometer *Laser Phys.* **28** 085107
[30] Li X, Zhu Y, Lin C, Zou C, Zhu Y, Dang F, Lin Y, Yuan Y and Yang J 2024 Performance improvement of a distributed temperature sensor with kilometer length and centimeter spatial resolution based on polarization-sensitive OFDR *Sens. Actuators A* **373** 115430
[31] Othonos A 1997 Fiber bragg gratings *Rev. Sci. Instrum.* **68** 4309–41
[32] Sun S, Mao Y, Deng M, Lan B and Jian C 2026 Research on fiber Bragg grating based composite sensing of flow velocity and temperature in oil immersed transformers *Meas. Sci. Technol.* **37** 015110
[33] Lu X 2016 Coherent Rayleigh time domain reflectometry: novel applications for optical fibre sensing *PhD Thesis* École Polytechnique Fédérale de Lausanne

[34] Lu X and Hicke K 2025 Error suppression in wavelength scanning coherent optical time domain reflectometry by polarization diversity detection *Measurement* **253** 117733

[35] Minardo A, Bernini R, Ruiz-Lombera R, Mirapeix J, Lopez-Higuera J and Zeni L 2016 Proposal of Brillouin optical frequency-domain reflectometry (BOFDR) *Opt. Express* **24** 29994–30001

[36] Renner E, Mampilli J, Amer N and Schmauss B 2024 Single-channel distributed Raman temperature sensing based on a 1-dimensional convolutional neural network *Opt. Fiber Technol.* **88** 104000

[37] Dey K, Inalegwu C O, Bartlett L, Jie R, Gerald E R, Zhu C and Huang J 2026 High-density fiber Bragg grating array enabling fully distributed sensing with sub-millimeter spatial resolution *Opt. Lett.* **51** 117–20

[38] Zhang X, Wang R, Bo W, Jin J, Zhang S, Liu K, Jiang J and Liu T 2025 Phase encoding for FBG code-division multiplexing sensing system in the ultrasonic frequency range *J. Lightwave Technol.* **43** 5156–65

[39] Jia J, Zhang J, Zhang T, Fu X, Jin W, Bi W and Fu G 2025 High spatial resolution distributed temperature and strain sensing based on current internal modulation DFB laser *Sens. Actuators A* **396** 117100

[40] Soto M and Thévenaz L 2013 Modeling and evaluating the performance of Brillouin distributed optical fiber sensors *Opt. Express* **21** 31347–66

Kishida K, Li C and Nishiguchi K 2005 Pulse pre-pump method for cm-order spatial resolution of BOTDA *Proc. SPIE* **5855** 559–62

[41] Wang H and Dai J 2019 Strain transder analysis of fiber Bragg grating sensor assembled composite structures subjected to thermal loading *Composites B* **162** 303–13

[42] Lu X, Soto M and Thévenaz L 2018 Impact of the fiber coating on the temperature response of distributed optical fiber sensors at cryogenic ranges *J. Lightwave Technol.* **36** 961–7

[43] Dey K, Kumer Saha R, Zhang B, Narasimman S, Mumtaz F, Smith J D, Gerald R E, O'Malley R J and Huang J 2026 Mitigating hysteresis in metal-coated fibers via optimized thermal treatment for advanced distributed high-temperature sensing applications *IEEE Trans. Instrum. Meas.* **75** 9502318

[44] Wang K, Schukar M, Hicke K and Lu X 2026 Effect of humidity on fiber-optic temperature sensing *Measurement* **261** 119905

[45] Lu X and Schukar M 2025 Humidity response of optical fibres with hygroscopic coatings and its temperature dependence *J. Phys. Photon.* **7** 025026

[46] Lindner E, Mörbitz J, Chojetzki C, Becker M, Brückner S, Schuster K, Rothhardt M and Bartelt H 2011 Draw tower fiber Bragg gratings and their use in sensing technology *Proc. SPIE* **8028** 80280C

[47] Leviton D and Frey B 2006 Temperature-dependent absolute refractive index measurements of synthetic fused silica *Proc. SPIE* **6273** 62732K